Optical investigation of carrier tunneling in semiconductor nanostructures

V. Emiliani,* S. Ceccherini, F. Bogani, and M. Colocci
Istituto Nazionale per la Fisica della Materia and European Laboratory for Nonlinear Spectroscopy, Dipartimento di Fisica, Largo E. Fermi 2, I-50125 Firenze, Italy

A. Frova
Istituto Nazionale per la Fisica della Materia, Dipartimento di Fisica, Universitá ''La Sapienza,'' Piazzale A. Moro, I-00198 Roma, Italy

Song Stone Shi
QUEST Center, University of California, Santa Barbara, California 93106
(Received 12 September 1996; revised manuscript received 29 January 1997)

The tunneling dynamics of excitons and free carriers in $Al_xGa_{1-x}As/GaAs$ asymmetric double quantum well and near-surface quantum well structures has been investigated by means of time-resolved optical techniques. The competing processes of carrier tunneling out of the quantum well and exciton formation and recombination inside the quantum well have been thoroughly studied in the range of the excitation densities relevant to device applications. A consistent picture capable of fully describing the carrier and exciton-tunneling mechanisms in both types of structures has been obtained and apparently contrasting results in the recent literature are clarified. [S0163-1829(97)01424-0]

I. INTRODUCTION

The photoluminescence (PL) signal from a quantum well (QW) sitting in the proximity of a real surface is strongly affected from the thickness of the surface barrier, Lb. In $Al_{0.3}Ga_{0.7}As/GaAs$ near-surface quantum well (NSQW) structures, the PL signal starts decreasing for Lb of the order of 12 nm and is nearly equal to zero for Lb less than 5 nm;[1] in $In_xGa_{1-x}As/GaAs$ ($x=0.1$–0.13) NSQW structures, due to the deeper wave-function penetration into the surface barrier, the PL signal starts decreasing for Lb of the order of 15 nm and drops to zero for Lb less than 9 nm.[2,3] It is generally agreed, by now, that the decrease of the PL intensity is due to the fact that carriers photogenerated in the well can tunnel to the surface states localized at the interface between the semiconductor surface and the surface oxide, with consequent loss in the radiative emission efficiency from the well. Detailed investigations of such tunneling processes and their dependence on the surface quantum well width, surface treatment, and sample material have been recently reported by many groups;[4–11] unfortunately, a clear picture of the observed phenomenology is still missing. In fact, it has been found that the dominant process in $Al_xGa_{1-x}As/GaAs$ involves tunneling of free carriers before binding into excitons, while a more complicated dynamics has been observed in $In_xGa_{1-x}As/GaAs$ (Ref. 11) where tunneling of carriers out of excitonic complexes has been found responsible for a shortening of the PL decay time as soon as the surface barrier is reduced below 10 nm, roughly.

On the other hand, similar tunneling processes through thin barriers have been extensively studied in asymmetric double quantum well (ADQW) systems;[12–22] in this case, carriers tunnel from one well to the other as long as the tunneling time is shorter than the recombination time, with tunneling rates mainly dependent on the position of the confined levels in the two wells and on the barrier width. Again, tunneling of free carriers or, rather, tunneling of excitonic complexes has been invoked by different groups in order to explain apparently contrasting experimental findings.

We want to show that a skillful use of complementary time-resolved PL techniques, based on a streak camera, on one side, for directly measuring the PL decay time at the heavy-hole exciton fundamental transition and on a PL excitation correlation technique[23–28] with subpicosecond time resolution, on the other, can indeed provide a consistent picture for the whole variety of tunneling processes occurring in both the NSQW and ADQW structures in the range of excitation densities particularly relevant to device operation.

We are able to determine separately the exciton formation, time, the tunneling times of the photogenerated carriers before and after exciton formation, and the exciton radiative recombination time, so as to fix all the free parameters of the rate-equation system describing the carrier tunneling dynamics. A very good agreement between the predictions of the model and the experimental data has been reached in very different experimental situations.

This paper is organized as follows. In Sec. II we will describe the samples and the experimental setup used in this work. We will briefly report in Sec. III the theoretical considerations needed for the analysis of the experimental data in the different experimental situations. In Sec. IV the experimental results are presented and the free parameters of the model are fitted to the experimental data. The results and the fit parameters are discussed in Sec. V. Finally, the conclusions are drawn in Sec. VI.

II. EXPERIMENT

The ADQW structure investigated is an undoped $Al_{0.3}Ga_{0.7}As/GaAs$ heterostructure grown by molecular beam epitaxy (MBE) on a Si-doped (100)-oriented GaAs substrate. The narrow well (NW), 3.1 nm in width, is sepa-

rated from the wide well (WW), 8.8 nm in width, by an $Al_xGa_{1-x}As$ barrier of $Lb=3.7$ nm. The NSQW structure investigated consists of two $Al_{0.3}Ga_{0.7}As/GaAs$ QW's grown by MBE on a nonintentionally doped GaAs substrate. The upper QW (hereafter called QW1), grown at distance Lb from the oxidized surface, is 3.5 nm in width and it is grown at a distance of 350 nm from a deeper QW (called hereafter QW2) 6 nm in width. Due to the large distance between the two wells, tunneling of carriers between the wells is absent. The deeply embedded well is insensitive to surface states and it is used as a reference well. Two different samples have been investigated, sample *A* and sample *B*, with Lb equal to 8 and 40 nm, respectively; in the latter, Lb is sufficiently thick to block carrier tunneling to surface states.

In order to characterize the samples, continuous wave (cw) PL and PL excitation (PLE) spectra have been performed using a Ti:sapphire tunable laser pumped by an Ar^+ ion laser. The spectra were recorded by a standard single photon-counting system after dispersion of the luminescence through a double spectrometer.

Time-resolved photoluminescence (TR PL) measurements were carried out at $\simeq 10$ K at the peak of the heavy-hole exciton band, using, for excitation, a dye laser that generated 6-ps-long pulses with a repetition rate of 76 MHz; the PL signal was dispersed through a 0.22-m double spectrometer and a synchroscan streak camera with an overall time resolution of about 20 ps was used for the detection. The excitation wavelength was 720 nm, corresponding to an excitation energy below the band gap of the barrier material ($Al_xGa_{1-x}As$); carriers were therefore photogenerated only in the wells. Before focusing onto the sample, $\simeq 10\%$ of the laser beam is diverted by a beam splitter and focused onto the entrance slit of the streak camera in order to acquire the instrumental response function of the system together with the PL signal.

The experimental setup used for the PL excitation correlation measurements has a standard configuration;[23–28] the ultrafast pulses are produced by a mode-locked Ti-sapphire laser pumped by an Ar^+ ion laser. The output consists in a train of pulses having a time duration of 130 fs, repetition rate $1/t_{\rm rep}$ of 80 MHz, and a wavelength of 720 nm. The pulse train is split into two beams of equal intensities and orthogonal polarizations; the path length of one of the beams can be changed, thus varying the delay time δ between the pulses; the relative delay (maximum delay ± 400 ps) is controlled by a programmable step motor. One of the beams is chopped at $f_1=311$ Hz, the other beam at $f_2=260$ Hz. The two collinear beams are then focused onto a 125-μm-diameter spot on the sample surface. The luminescence is collected and imaged onto the entrance slit of a 0.22-m double spectrometer. Finally the spectrally resolved PL signal is detected by a GaAs photomultiplier tube (PMT). After amplification the PMT signal is synchronously filtered by a lock-in amplifier at either one of the fundamental frequencies, f_1 or f_2, or at the sum frequency, $f_{\rm sum}=f_1+f_2$. Two kinds of measurements can be performed: it is possible to fix the detection frequency and acquire the signal as a function of the delay time δ or, in turn, to fix δ and scan the emission frequency. We will refer to the first one as *time-resolved correlation* (TRC) and to the second one as *frequency-resolved correlation* (FRC).

III. THEORETICAL CONSIDERATIONS

In order to describe the exciton dynamic in the presence of tunneling, we assume the following rate-equation system:

$$\begin{aligned}
\frac{dn}{dt} &= G(t,\delta) - Cnp - \frac{n}{\tau_e} + \frac{\nu}{\tau_{h\rm ex}}, \\
\frac{dp}{dt} &= G(t,\delta) - Cnp - \frac{p}{\tau_h} + \frac{\nu}{\tau_{e\rm ex}}, \\
\frac{d\nu}{dt} &= Cnp - \nu\left(\frac{1}{\tau_r} + \frac{1}{\tau_{e\rm ex}} + \frac{1}{\tau_{h\rm ex}}\right),
\end{aligned} \tag{1}$$

where n, p, and ν are the electron, hole, and exciton density at time t, respectively; τ_e and τ_h are the tunneling times for free electrons and holes, while the tunneling of an electron or a hole from an excitonic state, with the consequent production of a free carrier, is given by the rates $\nu/\tau_{e\rm ex}$ and $\nu/\tau_{h\rm ex}$; τ_r is the total residual exciton decay time including both radiative and nonradiative processes. Electrons and holes are assumed to have different tunneling times due to the difference in their effective masses and, for the NSQW structures, in the surface-state density available for the two types of carriers. $G(t,\delta)$ is the excitation term that is given by a single short pulse [i.e., $G(t,\delta)=G(t,0)$] when performing streak-camera measurements and by a pair of short pulses, delayed by δ, when performing correlation measurements. Finally the exciton formation at the excitation density used in this paper can be assumed to be bimolecular[29] and characterized by the coefficient C. It is evident from Eqs. (1) that free-carrier tunneling (n/τ_e, p/τ_h) is in competition with the exciton formation (Cnp) while tunneling of carriers coming from an excitonic state ($\nu/\tau_{e\rm ex}$, $\nu/\tau_{h\rm ex}$) competes with the exciton recombination ($1/\tau_r$) and gives rise to finite terms in the free carriers populations; in the following, carriers originating at an excitonic state will be called *excitonic carriers*.[27]

It should be noted that Eqs. (1) do not give a complete description of the exciton recombination dynamics; in fact, they do not take into account the exciton relaxation from the $k\neq 0$ states to the $k\simeq 0$ states allowed for radiative decay. However, as long as a time-integrated PL signal is detected, the simplified model of Eqs. (1) can be indeed used, as already discussed in Ref. 27. The point is that the PL signal is proportional to the time-integrated exciton population at $k=0$, which is in turn proportional to the time integral of the product np of the free-carrier populations. Since the time evolution of n and p is determined by the total exciton density, one can try to use a single equation for the global exciton population; within this picture, Eqs. (1) provide a simple modeling of the carrier dynamics, enough to interpret the result of the time-integrated measurements. Then, in Eqs. (1), ν is the total exciton density and the time constants and parameters have to be considered as average quantities over the global populations. As far as the PL time evolution is concerned Eqs. (1) fail to describe the dynamics of the $k=0$ excitons and a separate equation should be explicitly

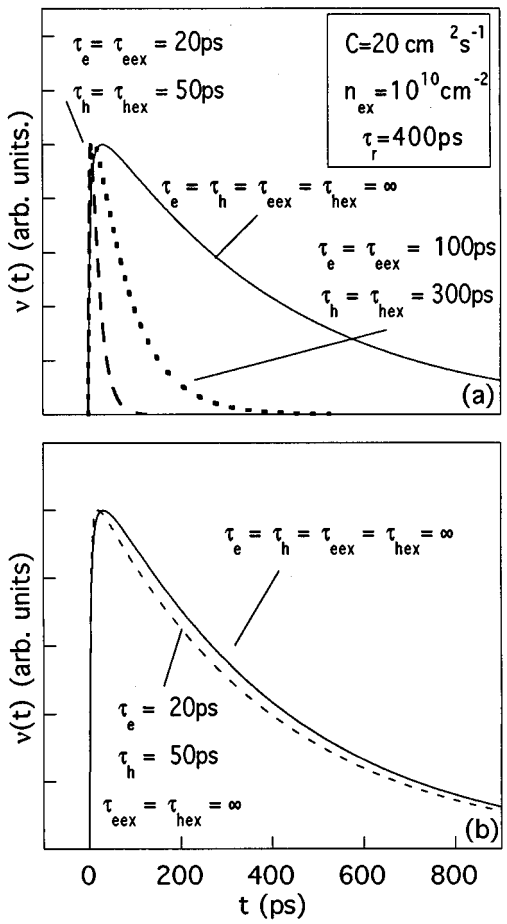

FIG. 1. Theoretical curves $\nu(t)$ calculated for the sets of parameters reported in the figure.

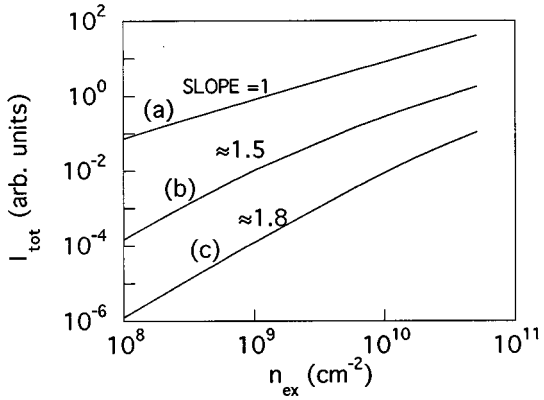

FIG. 2. Calculated curves $I_{\rm tot}$ as a function of $n_{\rm ex}$ with $\tau_r=400$ ps, $C=20$ cm^2 s^{-1} ($1/Cn_{\rm ex}=1$–500 ps), and (a) $\tau_e=\tau_{e\rm ex}=\tau_h=\tau_{h\rm ex}=\infty$, (b) $\tau_e=\tau_{e\rm ex}=20$ ps, $\tau_h=\tau_{h\rm ex}=50$ ps, (c) $\tau_e=\tau_{e\rm ex}=2$ ps, $\tau_h=\tau_{h\rm ex}=5$ ps.

added. However, it is easy to show that when the carrier tunneling rates prevail over the others the $k=0$ exciton population evolves according to a multiexponential law with a decay time mainly determined by the longest of the tunneling times. Then, since our work falls in this regime, we leave out the rate equation for the $k=0$ excitons and we stick to the simplified system (1); of course, proper consideration of the preceding statement has to be taken when the time-resolved PL measurements are discussed.

By solving the rate-equation system (1), the exciton density $\nu(t,n_{\rm ex},\delta)$ can be obtained as a function of the time, of the excitation density $n_{\rm ex}$, and of the delay δ. For $\delta=0$ and a fixed value for $n_{\rm ex}$ the calculated exciton density $\nu(t)$ is proportional to the TR PL intensity $I(t)$. Figures 1(a) and 1(b) show the curves $\nu(t)$, calculated with the set of parameters reported in the figures. If all the tunneling times were put equal to infinity [solid line Fig. 1(a)], the total exciton decay time would come out equal to τ_r. It is shorter than τ_r, instead, for finite values of the tunneling times (dashed and dotted line). Figure 1(b) shows that, if the tunneling of excitonic carriers is neglected and only tunneling of free carriers is considered, the total exciton decay time remains constant. The effect of changing the exciton-formation coefficient C (not shown here) is to slightly modify the rising part of the curve. This means that tunneling of free carriers and its competition with the exciton formation do not affect the decay time of the exciton luminescence, but at most they affect the rise time; therefore, a streak-camera measurement makes it possible to get information only on the competing processes of excitonic-carrier tunneling and exciton recombination, given the limited time resolution of the order of 15–20 ps, much too large for a reliable determination of short rise times (typically a few tens of ps at most).

By time integrating the calculated expression $\nu(t,\delta,n_{\rm ex})$, the two-pulse intensity $I_{\rm tot}(\delta,n_{\rm ex})$ can be obtained both as a function of the excitation intensity $n_{\rm ex}$ (at fixed δ) and as a function of the delay δ (at fixed $n_{\rm ex}$).

In Fig. 2 the function $I_{\rm tot}(n_{\rm ex})=I_{\rm tot}(n_{\rm ex},\delta=0)$, equivalent to the single pulse time integrated PL, is plotted on a log-log scale for the set of parameters reported in the figure caption. As shown in the Appendix, as long as carrier tunneling occurs and the exciton formation is a bimolecular process, $I_{\rm tot}(\delta,n_{\rm ex})$ turns out to be a superlinear function of the excitation density, being quadratic in the limiting case where tunneling of free carriers is the dominant recombination mode [Eq. A4]. What strongly affects the slopes of the curves is the relation between the product $Cn_{\rm ex}$ and the faster tunneling rates; as a matter of fact the superlinear dependence on $n_{\rm ex}$ is a consequence of the competition between the exciton-formation time $1/Cn_{\rm ex}$ (inversely proportional to $n_{\rm ex}$) and the tunneling of free carriers (independent of $n_{\rm ex}$).[3,27]

Finally, the expression

$$I_{\rm nl}=I_{\rm tot}(\delta,n_{\rm ex})-2I, \tag{2}$$

where $I=I(\delta=\infty,n_{\rm ex})$ is the luminescence originated by a single pulse, can be calculated at a fixed value of $n_{\rm ex}$ and corresponds to the correlation signal. As far as $I_{\rm tot}$ is a superlinear function of $n_{\rm ex}$, the expression (2) is different from zero and depends on the delay δ between the pulses [Eq. A4]. In Figs. 3(a)–3(c), the function (2) is plotted, normalized to the maximum, for the sets of parameters shown in the figures. If only tunneling of free carriers were considered [Fig. 3(a)], a fast decay followed by a slower one should be observed, the discontinuity between the two different slopes depending on the excitation intensity [Fig. 3(b)] and on the difference between the two tunneling times. If also tunneling

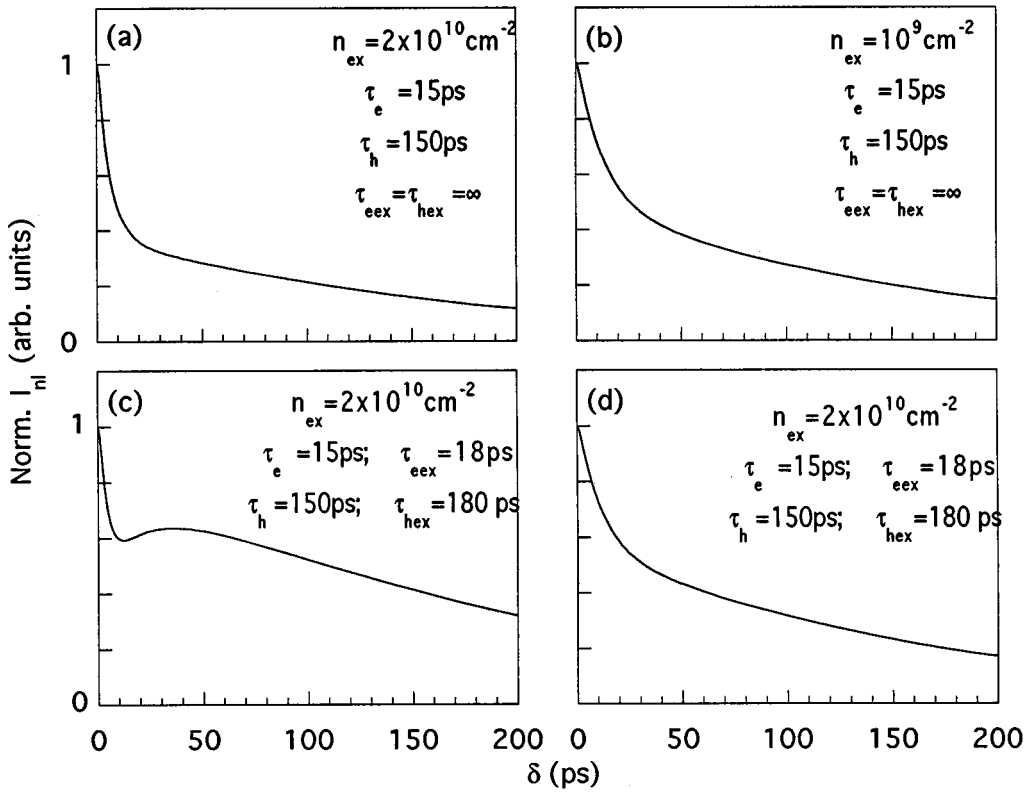

FIG. 3. Normlized calculated curves $I_{\rm nl}=I_{\rm tot}-2I$ for the sets of parameters reported in the figure.

from excitonic carriers were effective, a very characteristic behavior should appear, as illustrated in Fig. 3(c). The initial decay depends on the competition between the exciton formation and the tunneling of the faster free carrier; the shoulder is due to the tunneling of the faster excitonic carriers, which leaves the other carrier in the well that possibly forms an exciton again. Finally the slower decay is due to the tunneling of the slower, free or excitonic, carrier. The amplitude of the shoulder depends on the excitation intensity [Fig. 3(d)]; as a matter of fact the higher the excitation intensity, the faster the exciton formation time, and the excitonic carriers left in the well will form again excitonic complexes instead of tunneling out of the well. The PL excitation correlation technique allows one to measure a signal proportional to $I_{\rm nl}$.

In summary, the TR PL measurements are sensitive to the total exciton decay and allow one to determine, in no-tunneling samples, the value of τ_r; the PL dependence on $n_{\rm ex}$ is sensitive to the competition between free-carrier tunneling and exciton formation; finally, the correlation measurements allow one to emphasize the presence of different tunneling times for electrons and holes, both for free and for excitonic carriers. By fitting the data obtained from the different experiments, it is thus possible to deduce the values of all the time constants involved in the process.

IV. RESULTS

A. Asymmetrical double quantum well structure

In Fig. 4 the PL spectrum of the ADQW structure is reported together with the PLE spectrum of the WW. The two peaks in the PL spectrum at 743 and 794 nm correspond to the heavy-hole exciton recombination in the NW and WW, respectively. The PLE spectrum of the WW (detection energy 797.2 nm) shows that tunneling occurs from the narrow to the wide well. In fact clearly resolved structures corresponding to the heavy- and light-hole ($e1$hh1, $e$llh1) exciton transitions from the NW are present in addition to the light-hole and heavy-hole ($n=2$), exciton transitions ($e1$lh1′, $e2$hh2′) coming from the WW. We also note that a Stokes shift of the order of 3 meV is measured in both wells, as usually found in good quality QW's of similar thickness.

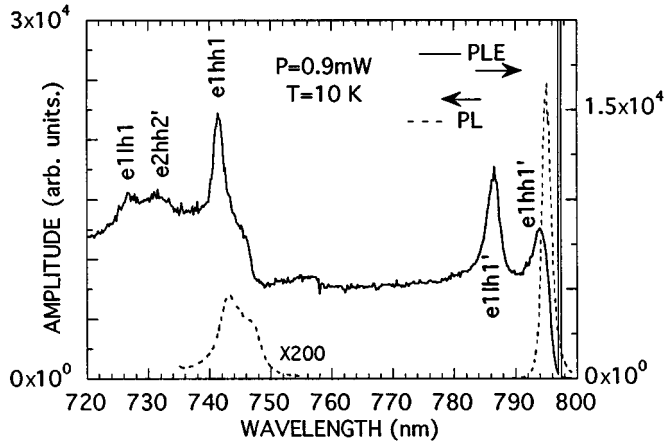

FIG. 4. PL spectra (dashed line) from the NW and WW of the ADQW structure and PLE spectrum (solid line) from the WW of the ADQW sample; the excitation wavelength of the PL spectrum is 720 nm.

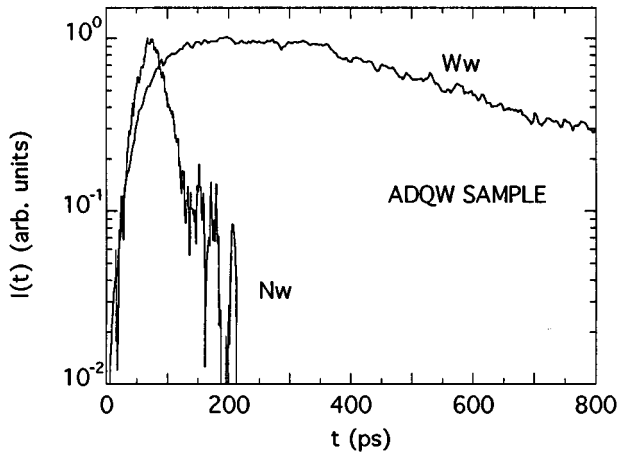

FIG. 5. Heavy-hole exciton decay curves from the NW and WW of the ADQW; $n_{ex} \simeq 10^{10}$ cm^{-2}, $T = 10$ K, and $\lambda_{exc} = 720$ nm.

In Fig. 5 the temporal decay of the luminescence signal at the fundamental exciton transitions in the two wells is reported; we note that the decay time of the PL from the NW is very fast in comparison with the decay time from the WW. This suggests that, in the NW, exciton tunneling (as a neutral or charged particle) is in strong competition with its radiative recombination.

Figure 6 shows, in a log-log scale, the spectrally integrated luminescence as a function of n_{ex} for the heavy-hole exciton band from the two wells. The slopes of the two curves are $\simeq 1$ and $\simeq 1.4$, respectively, for WW and NW, confirming, in the latter case, the superlinear dependence on n_{ex} predicted when tunneling of free carriers occurs. It should be noted that the slope of the time-integrated PL from WW is slightly less than 1, indicating that saturation effects are present. This is in agreement with the observed Stokes shift between the PL and PLE peak of the $e1hh1'$ recombination shown in Fig. 4, suggesting recombination from localized excitons.

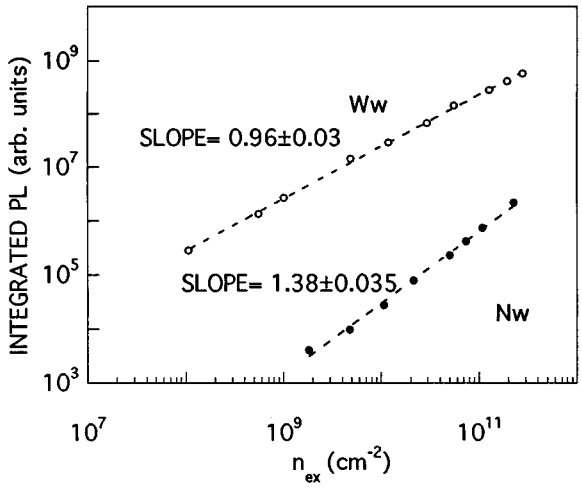

FIG. 6. Spectrally integrated luminescence intensity as a function of n_{ex} for the two wells of the ADQW sample, $T = 10$ K, and $\lambda_{exc} = 721$ nm.

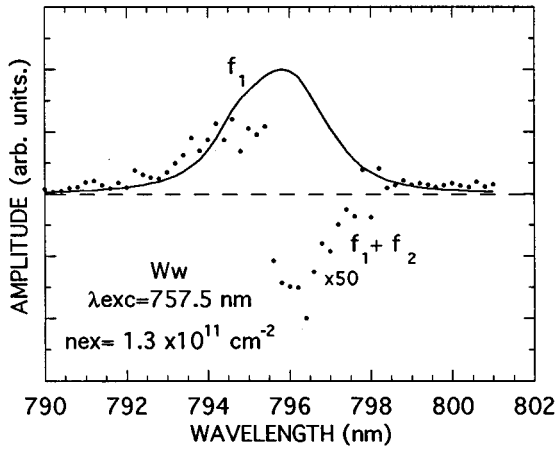

FIG. 7. Fundamental (solid line) and sum frequency (dots) spectra from the WW of the ADQW sample for $n_{ex} \simeq 10^{11}$ cm^{-2}. The amplitudes of the signals are normalized to the maximum value.

In Fig. 7 the FRC signal, I_{sum}, at the sum frequency $f_1 + f_2$ and at delay $\delta = 0$ from WW is compared to the corresponding FRC signal at the fundamental frequency f_1.[30] Due to the saturation of the bound-exciton state, the signal I_{sum} on the low-energy side of the spectrum is negative (sublinear) while it becomes positive (superlinear) on the high-energy side. Anyway, this signal is at most 2% of that at the fundamental frequency and thus exciton recombination from WW can be considered as a linear recombination process with a good approximation.

In Fig. 8 we report the FRC at the sum frequency ($\simeq 10\%$ of signal at the fundamental frequency) and the FRC spectrum at the fundamental frequency f_1 from NW. In this case the good coincidence between the two spectra confirms that the signal has the same dependence on n_{ex} for all energies of the recombination band and no strong dynamics, which could affect the correlation spectra, are present within the band; tunneling to the WW is the dominant process and the exciton recombination band has a superlinear dependence on n_{ex}.

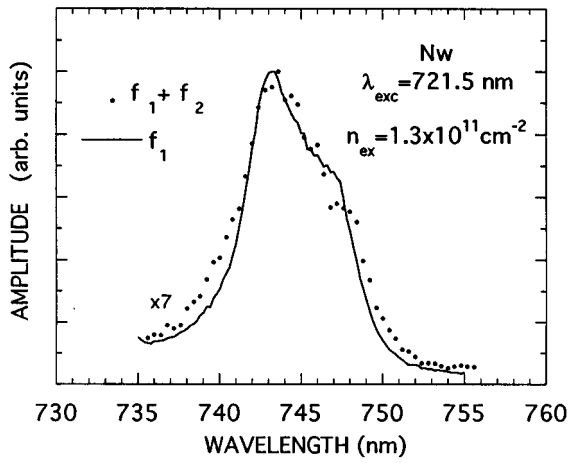

FIG. 8. Fundamental (solid line) and sum frequency (dots) spectra from the NW of the ADQW sample for $n_{ex} \simeq 10^{11}$ cm^{-2}. The amplitudes of the signals are normalized to the maximum value.

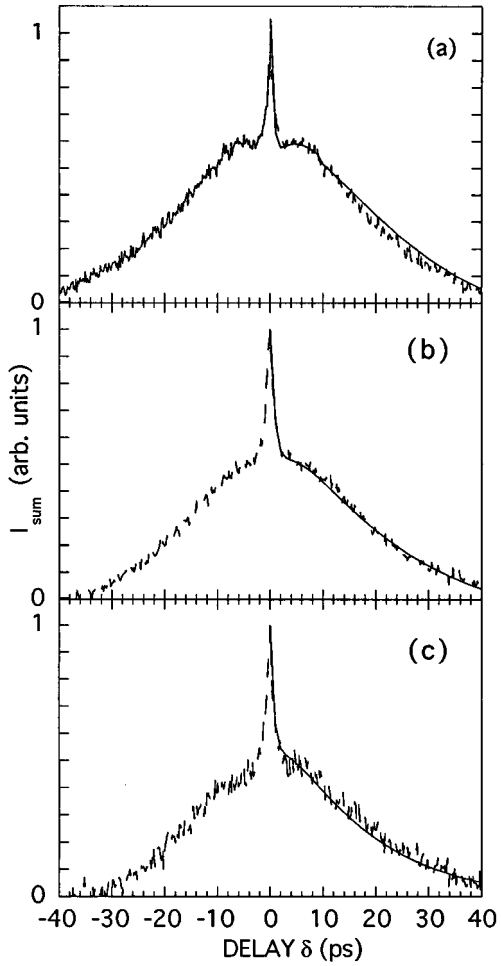

FIG. 9. Normalized sum frequency signal vs delay from the NW of the ADQW sample and relative curve fit (solid line) at (a) $n_{ex}=3\times10^{11}$ cm^{-2}, (b) $n_{ex}=1.4\times10^{11}$ cm^{-2}, (c) $n_{ex}=5\times10^{10}$ cm^{-2}.

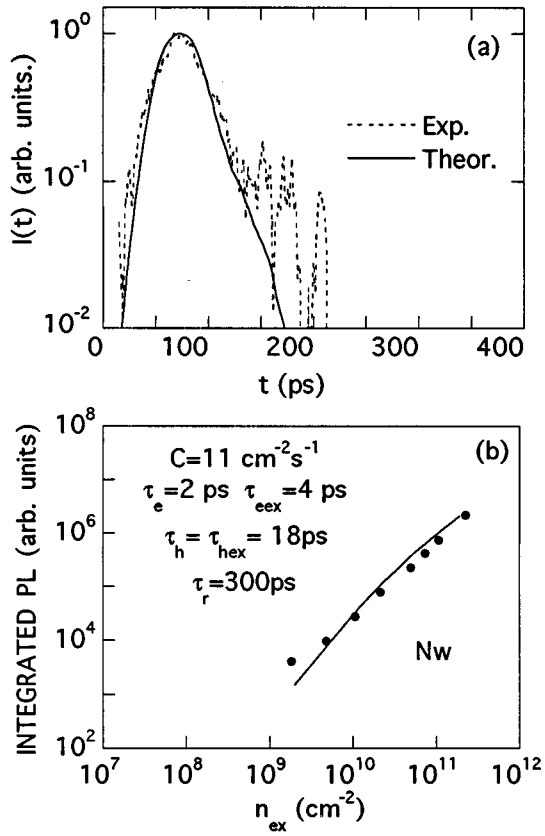

FIG. 10. TR and spectrally integrated PL data of Figs. 5 and 6 compared to the theoretical curves calculated from the rate-equation system (1) with the set of parameters reported in the figure.

In Fig. 9 the TRC signal from the NW obtained at f_1+f_2 is plotted as a function of the delay δ between the two pulses for different excitation densities. Three distinct regions can be distinguished: the first fast-decay region (0–4 ps) governed by exciton formation and tunneling of the faster tunneling carrier; the bump at intermediate times (4–10 ps) due to the carriers left in the well after the breaking of the exciton (whose amplitude depends on the excitation density) and, finally (10–50 ps), a long time constant decay due to tunneling of the slower carriers. Also shown is the best fit to the data obtained with the model described in the previous section. The parameters used to fit the experimental curves of Fig. 9 are reported in Table I; the exciton decay time τ_r is fixed at the value determined by the PL decay time at the WW heavy-hole exciton transition energy as measured by the streak camera (Fig. 7).

It is important to stress that the set of parameters reported in Table I were determined by performing the best fit to the three independent measurements, i.e., the TRC signal, the TR-PL measurements, obtained with the streak camera, and the PL dependence on the carrier density. The best fits to $I(t)$ (Ref. 31) and I_{tot} are shown in Figs. 10(a) and 10(b), together with the experimental data. Note once again that, in spite of the rather large number of free parameters in Eqs. (1), strong confidence has to be given to the values obtained, given the constraints imposed by fitting experimental data taken in different kinds of experiments with the same set of parameters.

B. Near surface quantum well structures

As stated in Sec. II, two different NSQW structures were examined, sample *A* and sample *B*, which only differ in the value of *Lb* (8 and 40 nm, respectively). Sample *B* is used as a reference no-tunneling sample. The PL and PLE spectra of the two wells of sample *A* after cw excitation are reported in

TABLE I. Set of parameters used to calculate the solid lines in Fig. 9.

C (cm^2 s^{-1})	τ_e (ps)	τ_h (ps)	τ_{eex} (ps)	τ_{hex} (ps)	τ_r (ps)	n_{ex} (cm^{-2})
11±2	1±0.5	18±1			300±10	≃5×10^{10}
9±2	2±0.5	19±1	4±2	18±2	300±10	≃1.3×10^{11}
12±2	2±0.5	18±1	4±0.5	18±2	300±10	≃2.8×10^{11}

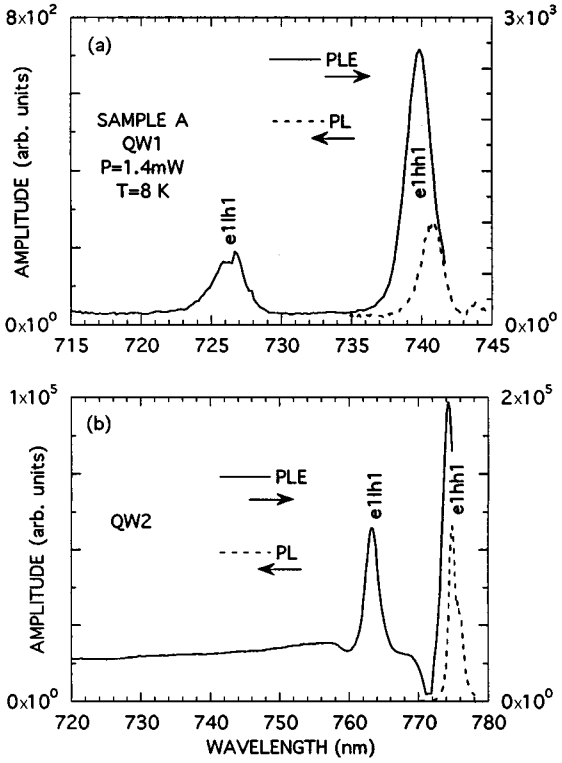

FIG. 11. PL (dashed line) and PLE spectra at 10 K (solid line) from (a) QW1 and (b) QW2 of sample A. The excitation energy of the PL spectra is 720 nm.

Figs. 11(a) and 11(b), respectively. Structures corresponding to transitions in the QW1 are not observed in the PLE of QW2 and vice versa, confirming that charge transfer between the wells can be neglected. In both QW's a small Stokes shift is present between the PL and PLE heavy-hole peaks (e1hh1).

Figure 12 shows that, as a consequence of the competition between tunneling of free carriers and exciton formation, the spectrally integrated heavy-hole exciton band from QW1 of sample A is a superlinear function of n_{ex}; on the contrary, it is a linear function of n_{ex} in the case of QW1 of sample B and QW2 of both samples (not shown here).

In Figs. 13(a) and 13(b) the time evolution of the heavy-hole line from both QW1 and QW2 of samples A and B is plotted. It is evident that, when no tunneling to surface states occurs (QW1 of sample B and QW2 of both samples), the decay time is of the order of a few hundred ps, while it gets shorter in the case of the exciton recombination from QW1 of sample A. It is important to underline that this result strongly depends on the well width, at least in $Al_xGa_{1-x}As/GaAs$ NSQW structures. As a matter of fact, the exciton decay time remains constant for widths of QW1 of 6 and 10 nm up to surface barrier thicknesses of 3 nm:[10,11] the well width strongly influences the free carrier and exciton wave-function penetration into the barrier, which is deeper the thinner the well width, causing the tunneling time τ_{eex} and τ_{hex} and thus the total exciton decay time to become shorter.

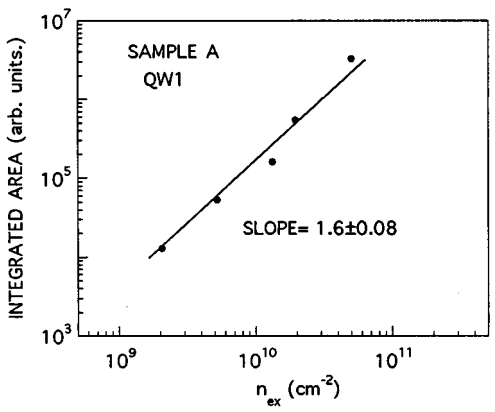

FIG. 12. Spectrally integrated luminescence intensity as a function of n_{ex} for the QW1 of sample A; $T=10$ K, $\lambda_{exc}=$ 720 nm.

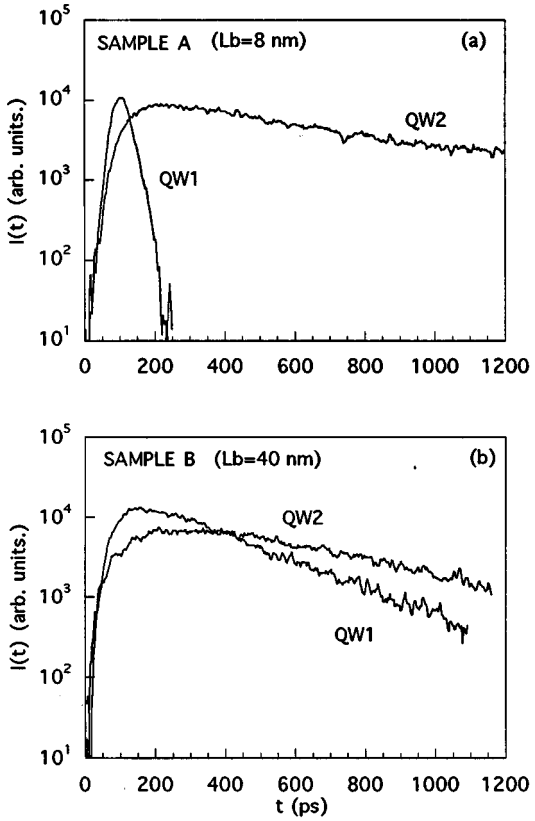

FIG. 13. Heavy-hole exciton decay curves from QW1 and QW2 of (a) sample A and (b) sample B. $n_{ex}\simeq 2\times 10^9$ cm^{-2}, $T=10$ K, and $\lambda_{exc}=$ 720 nm.

In Figs. 14(a) and 14(b) the FRC at frequencies f_1+f_2 and f_1 are plotted for the two wells.[30] The sum frequency signal from QW2 is positive or negative (i.e., superlinear or sublinear) depending on the detection energy; this points to an internal band dynamics due to the saturation of the localized exciton states, whose presence has been suggested by the Stokes shift shown by the spectra in Fig. 11. Anyway, the sum frequency signal is only 3% of the signal at f_1, so that the exciton recombination band can be considered as having a linear dependence on n_{ex}. On the contrary, the sum frequency signal from QW1 (14% of the signal at f_1) is positive at all energies within the PL band and coincides with the spectrum at f_1; this shows that the PL is superlinear on n_{ex}

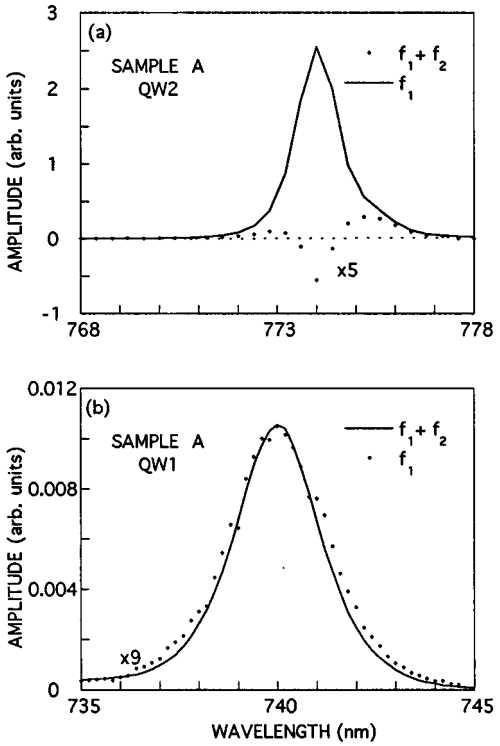

FIG. 14. Fundamental (solid line) and sum (dots) frequency spectra from (a) QW2 and (b) QW1 of sample A; $n_{ex} \simeq 3 \times 10^{10}$ cm^{-2}.

throughout the whole spectrum. The agreement between the spectra taken at the sum frequency and at f_1 keeps good also by varying the delay δ between the pulses (spectra not shown here), thus demonstrating that the TRC sum frequency signal does not depend on the detection energy. Finally, we report in Fig. 15 the TRC sum frequency signal detected at the heavy-hole exciton peak as a function of the delay between the pulses with the corresponding best fit. Again, three temporal regions can be distinguished: the first in the range 1–10 ps, the second, very evident, in the range 10–100 ps, and the last one in the range 100–300 ps. The fit parameters are reported in Table II.

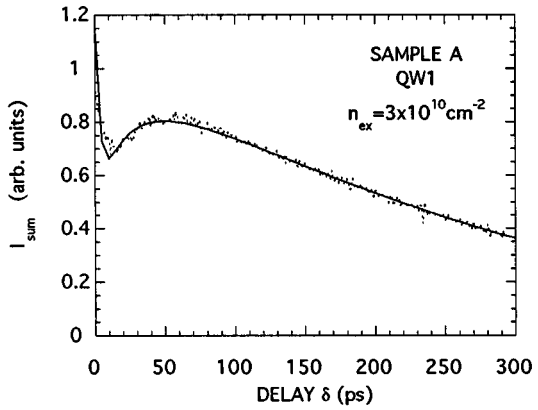

FIG. 15. Sum frequency signal vs delay detected at the heavy-hole exciton recombination peak from QW1 of sample A.

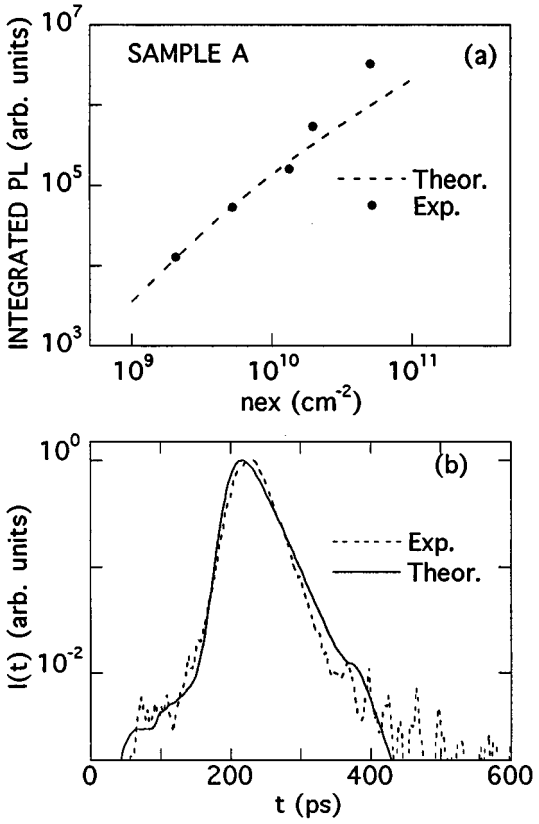

FIG. 16. Spectrally integrated PL and TR data of Figs. 12 and 13 compared to the theoretical curves calculated from the rate-equation system (1) with the set of parameters reported in Table II.

Also in this case, as shown in Fig. 16, we are able to reproduce, with the same set of parameters, the TR measurements $I(t)$ (Ref. 31) and the characteristic nonlinear dependence of I_{tot} on n_{ex}.

C. Saturation effects

In using the rate-equation system (1) to fit the experimental data the assumption has been made that the tunneling times do not depend on δ. This means that carriers photogenerated from the delayed pulse are assumed to tunnel with the same tunneling rates as the carriers photogenerated from the first pulse; that is, no saturation effects occur.

In the ADQW structures this is certainly a good approximation; the spectrally integrated PL from WW is indeed a linear function of n_{ex}, indicating that no band filling occurs. In the case of tunneling to surface states, this assumption has to be verified; carriers undergoing a fast tunneling process might saturate the surface states available to the tunneling of carriers photogenerated by the delayed pulse. As a consequence, the decay time of the PL signal coming from the excitonic recombination induced by the delayed pulse should be longer with respect to the decay time of the exciton luminescence induced by the first pulse.

In order to check this assumption, the laser beam has been divided into two equal beams, with one of the beams being delayed with respect to the other. The two beams were then collimated and focused onto the sample. We find that the time-resolved PL signals induced by the two beams repro-

TABLE II. Set of parameters used to calculate the solid line in Fig. 15.

C ($cm^2\ s^{-1}$)	τ_e (ps)	τ_h (ps)	τ_{eex} (ps)	τ_{hex} (ps)	τ_r (ps)	n_{ex} (cm^{-2})
20 ± 5	200 ± 10	11 ± 1	350 ± 30	25 ± 5	250 ± 5	$\simeq 3\times10^{10}$

duce the sum of the PL signals measured by blocking alternatively either beam, independently of the time delay. We conclude that the tunneling times can be considered independent of δ with a good approximation.

V. DISCUSSION

Let us start by discussing the values obtained for the bimolecular exciton formation coefficient C. Actually, very scarce information is available in the literature: to our knowledge, the only two papers reporting an explicit estimate for the coefficient C are Ref. 27, where a value of $C=6$ $cm^2\ s^{-1}$ has been used for fitting the experimental data in a $GaAs/Al_xGa_{1-x}As$ ADQW structures, and Ref. 32, where a value of $C\geqslant 14$ $cm^2\ s^{-1}$ is given for a shallow confined $In_xGa_{1-x}As/GaAs$ QW system. In both references the carrier density varies in the range 10^9–10^{10} cm^{-2}, roughly one order of magnitude less than the characteristic carrier densities used in our measurements, ($n_{ex}\simeq 10^{10}$–10^{11} cm^{-2}). Nevertheless, our data for C, ranging between $\simeq 10$ and 20 $cm^2\ s^{-1}$, are completely consistent with the values reported in both Ref. 27 and Ref. 32; these values imply an exciton formation time as short as $\simeq 10$ ps for a carrier density around 10^{10} cm^{-2}, in excellent agreement with the estimate of less than 20 ps reported in Ref. 33.

Let us now examine the carrier tunneling times. It has been customary, when discussing the nonresonant tunneling times in ADQW structures, to assume that the faster tunneling time has to be attributed to the free electrons due to their lighter effective mass. In this case, however, for the excitation energy used, as a consequence of valence-band mixing the hh1 state of the NW crosses the hh2′ state of the WW out of $k=0$. It is very likely, therefore, that the faster tunneling time in ADQW structures should be attributed to the holes.

As far as the NSQW structure is concerned, the parameter that strongly affects the tunneling probability is the surface-state density available for the two types of carriers. Two different models can be assumed for the surface-state distribution on GaAs real surfaces: the advanced unified defect model[34] (AUDM) and the disordered induced gap states (DIGS) model.[35] According to the first one, the surface-state density is mainly due to defects (Ga_{As} and As_{Ga}) energetically localized between the valence-band maximum and the midgap; holes could thus tunnel faster than electrons. The DIGS model predicts a U-shaped surface-state distribution, in this case tunneling of electrons is faster than tunneling of holes due to their less effective mass. We are not able to discriminate between these two opposite situations.

For both types of structures the excitonic tunneling times are slightly different from free-carrier tunneling times. In previous works we have found that for NSQW with a well width of 6 (Refs. 10 and 11) and 8 nm (Ref. 36) the tunneling to surface states is totally dominated by free carriers; excitonic carriers are, on the contrary, strongly confined in the well and their corresponding tunneling times are infinity. This is in agreement with the observation that, due to the Coulomb interaction, carriers bound in an excitonic state are more confined in the well than free carriers, thus experiencing longer tunneling times.[37,38]

Using a simple model of escape time[39] to calculate the tunneling times, it is possible to estimate the ratio between the tunneling times through barriers 8 and 3.7 nm thick; we find a ratio $\simeq 10^2$ and $\simeq 10^4$ for electrons and holes, respectively. By comparing the correspondent fit parameters obtained for the two structures (Tables I and II) we note that even if all the tunneling times in the NSQW ($Lb=8$ nm) structure are longer with respect to the case of the ADQW structure ($Lb=3.7$ nm), they still are of the same order of magnitude. We have to conclude that, due to a different state distribution, both in energy and in density, tunneling to surface states is strongly favorite compared to tunneling to confined states in a different QW, as confirmed by the fact that when the surface barrier thickness of a NSQW is reduced below 8 nm the PL from the QW rapidly goes to zero.

VI. CONCLUSIONS

The carrier tunneling dynamics in ADQW and NSQW structures has been investigated by time-resolved measurements.

We have shown that, while the straightforward measurement of the PL decay times makes it possible to give evidence for the competition between tunneling and exciton recombination, no direct distinction can be made between processes where excitons tunnel as a whole entity rather than as free-carriers, after exciton breaking. In fact, both mechanisms result in a decrease of the total exciton decay time.

The nonlinear dependence on the excitation energy of the PL signal when carrier tunneling is effective has allowed us to use a PL excitation correlation technique capable of discriminating between the two mechanisms and monitoring the competition between free-carrier tunneling and exciton formation.

We have shown that a joint analysis of the experimental data obtained with the two TR techniques and the excitation density dependence of the exciton emission band has allowed us to obtain all the time constants involved in the tunneling processes both to confined and to surface states.

Finally, tunneling to surface states has been found to be more efficient than that to confined states, with possible consequences for device application.

ACKNOWLEDGMENTS

We wish to thank Dr. A. Vinattieri and Dr. B. Bonanni for helpful discussions. Work at LENS has been supported by the ECC Contract No. GE1*CT92–0046.

APPENDIX

As shown in the text, in order to describe the excitonic recombination in the presence of tunneling mechanisms, we have assumed Eqs. (1). In our case the response of the samples is fast enough that adjacent pulses from the same train do not interact and the system goes to the equilibrium condition in a time less than $t_{\rm rep}$. We will thus consider the response of the system to a generation term expressed as the sum of two delayed pulses:

$$G(t,\delta)=\frac{1}{\sqrt{\pi}\tau_p}\left\{n_{\rm ex1}\exp\left[-\left(\frac{t}{\tau_p}\right)^2\right]+n_{\rm ex2}\exp\left[-\left(\frac{t-\delta}{\tau_p}\right)^2\right]\right\}, \tag{A1}$$

where $n_{\rm ex1,2}$ are the excitation densities of the two beams given by

$$n_{{\rm ex}i}=\alpha W J_i/(A_{\rm spot}h\nu), \tag{A2}$$

where α is the absorption coefficient, W the well width, and J_i, $h\nu$, and $A_{\rm spot}$ the pulse energy, the excitation-photon energy, and the area of the laser beam spot on the sample, respectively.

We will consider first two limiting cases.

If no tunneling occurs, $\tau_e=\tau_h=\tau_{e\rm ex}=\tau_{h\rm ex}=\infty$ and the equations become

$$\frac{dn}{dt}=\frac{dp}{dt}=G(t,\delta)-Cnp,\quad \frac{d\nu}{dt}=Cnp-\frac{\nu}{\tau_r}.$$

Integrating over the detector response (the corresponding time constant is long compared with the pulse duration τ_p), applying the condition that n, p, and ν over long time return to their steady-state value and putting in the effects of repetitive pulses, we obtain for the intensity of the exciton recombination

$$\begin{aligned}I_{\rm tot}&=\eta/t_{\rm rep}\int\frac{\nu}{\tau_r}dt=\eta/t_{\rm rep}\int Cnp\,dt=\eta/t_{\rm rep}\int G(t,\delta)dt\\&=\eta(n_{\rm ex1}/t_{\rm rep}+n_{\rm ex2}/t_{\rm rep})=I_1+I_2,\end{aligned} \tag{A3}$$

where η is the experimental efficiency and $I_{1,2}$ is the photoluminescence induced by a single pulse. For $n_{\rm ex1}=n_{\rm ex2}=n_{\rm ex}$, one has $I_1=I_2=I$ and $I_{\rm tot}=2I$. $I_{\rm tot}$ is a linear function of $n_{\rm ex}$ and does not depend on the delay δ, so that $I_{\rm nl}=I_{\rm tot}-2I=0$. Therefore the FRC spectra at frequency f_1+f_2 is zero and in addition the excitonic recombination has a linear dependence on $n_{\rm ex}$. In the other limiting case where tunneling of free carriers is the dominant recombination mode, Eqs. (1) become

$$\frac{dn}{dt}\simeq G(t,\delta)-\frac{n}{\tau_e},\quad \frac{dp}{dt}\simeq G(t,\delta)-\frac{p}{\tau_h},\quad \frac{d\nu}{dt}=Cnp-\frac{\nu}{\tau_r}.$$

From the first two equations we obtain (approximating the pulses by δ functions)

$$n(t)=n_{\rm ex1}\theta(t)e^{-t/\tau_e}+n_{\rm ex2}\theta(t-\delta)e^{-(t-\delta)/\tau_e},$$

$$p(t)=n_{\rm ex1}\theta(t)e^{-t/\tau_h}+n_{\rm ex2}\theta(t-\delta)e^{-(t-\delta)/\tau_h},$$

where $\theta(t)$ is the step function (equal to zero for times less than the argument and equal to one for longer times). Forming the Cnp product, integrating over the detector response, and including again the effect of pulse repetition, we obtain

$$\begin{aligned}I_{\rm tot}&=\eta/t_{\rm rep}\int\frac{\nu}{\tau_r}dt\\&=(\eta C/t_{\rm rep})[n_{\rm ex1}^2\tau+n_{\rm ex2}^2\tau+n_{\rm ex1}n_{\rm ex2}\tau(e^{-|\delta|/\tau_e}+e^{-|\delta|/\tau_h})]\\&=I_1+I_2+(\eta C/t_{\rm rep})[n_{\rm ex1}n_{\rm ex2}\tau(e^{-|\delta|/\tau_e}+e^{-|\delta|/\tau_h})],\end{aligned} \tag{A4}$$

where τ is the parallel between the tunneling times τ_e,τ_h; $I_{\rm tot}$ is a superlinear function of the excitation density (quadratic for $n_{\rm ex1}=n_{\rm ex2}$); the carrier's population induced by the two pulses interact making the term $I_{nl}=(C/t_{\rm rep})[n_{\rm ex1}n_{\rm ex2}\tau(e^{-|\delta|/\tau_e}+e^{-|\delta|/\tau_h})]$ different from zero and dependent on the delay δ.

In the intermediate cases the rate-equation system (1) can be solved numerically and $I_{\rm nl}$ is found to have a nonlinear dependence on the excitation density with an exponent between 1 and 2. If a lock-in technique is used to extract $I_{\rm nl}$, the two beams are then chopped at two different frequencies, f_1, f_2, and Eqs. (A3) and (A4), become

$$I_{\rm tot}=\eta[n_{\rm ex1}c(f_1,t)/t_{\rm rep}+n_{\rm ex2}c(f_2,t)/t_{\rm rep})], \tag{A5}$$

$$\begin{aligned}I_{\rm tot}=\eta(C/t_{\rm rep})[&n_{\rm ex1}^2c(f_1,t)\tau+n_{\rm ex2}^2c(f_2,t)\tau\\&+n_{\rm ex1}n_{\rm ex2}c(f_1,t)c(f_2,t)\tau(e^{-|\delta|/\tau_e}+e^{-|\delta|/\tau_h})],\end{aligned}$$

where $c(f_i,t)$ is the modulation function of the chopper.

It is thus possible to select the sum (or difference) frequency signal,

$$I_{\rm sum}=I(f_1\pm f_2)\propto\eta(C/t_{\rm rep})n_{\rm ex1}n_{\rm ex2}\tau(e^{-|\delta|/\tau_e}+e^{-|\delta|/\tau_h}),$$

that is proportional to the nonlinear part $I_{\rm nl}$ of the signal.

It is important to note that the signal $I_{\rm nl}$ is a function both of the delay δ and of the detection energy ϵ:

$$I_{\rm nl}(\epsilon,\delta)=I_{\rm tot}(\epsilon,\delta)-2I(\epsilon), \tag{A6}$$

and it is clear that, depending on whether the response of the sample is a superlinear or a sublinear function of $n_{\rm ex}$, the function (A6) is positive or negative.

If the PL dependence on $n_{\rm ex}$ is the same at all energies within the recombination band, the function (A6) reproduces (apart from the sign) the PL spectrum. On the contrary, function (A6) may change sign in the spectrum, and the correlation signal may strongly depend on the detection energy in this case.

*Now at the Physic Department of the University of Tor Vergata, Via della Ricerca Scientifica I-1033, Roma, Italy. Electronic address: emiliani@roma2.infn.it

[1] Y.-L. Chang, I. H. Tan, Y.-H. Zhang, J. Merz, E. Hu, A. Frova, and V. Emiliani, J. Appl. Phys. **62**, 2697 (1993).

[2] Y.-L. Chang, I.-H. Tan, Y.-H. Zhang, D. Bimberg, and J. Merz, J. Appl. Phys. **74**, 5144 (1993).

[3] V. Emiliani, B. Bonanni, A. Frova, M. Capizzi, F. Martelli, and

S.-S. Stone, J. Appl. Phys. **77**, 5712 (1995).
[4] J. M. Moison, K. Ecless, F. Houzay, J. Y. Marzin, J. M. Gérard, F. Barthe, and M. Bensoussan, Phys. Rev. B **41**, 12 945 (1990).
[5] Z. Sobiesierski, D. I. Westwood, D. A. Woolf, T. Fuki, and H. Hasegawa, J. Vac. Sci. Technol. B **11**, 1723 (1993).
[6] Y.-L. Chang, I.-H. Tan, E. Hu, J. Merz, V. Emiliani, and A. Frova, J. Appl. Phys. **75**, 3040 (1994).
[7] J. Dreybrodt, F. Daiminger, J. P. Reithmaier, and A. Forchel, Phys. Rev. B **51**, 4657 (1995).
[8] Y.-L. Chang, M. Krishnamurthy, I.-H. Tan, E. Hu, J. Merz, P. Petroff, A. Frova, and V. Emiliani, J. Vac. Sci. Technol. B **11**, 1702 (1993).
[9] Y.-L. Chang, I.-H. Tan, C. Reave, J. Merz, E. Hu, S. DenBaars, A. Frova, V. Emiliani, and B. Bonanni, Appl. Phys. Lett. **64**, 2658 (1994).
[10] V. Emiliani, B. Bonanni, C. Presilla, M. Capizzi, A. Frova, Y.-L. Chang, I. H. Tan, J. Merz, M. Colocci, and M. Gurioli, J. Appl. Phys. **75**, 5114 (1994).
[11] B. Bonanni, M. Capizzi, R. Dioletta, V. Emiliani, A. Frova, C. Presilla, M. Colocci, M. Gurioli, A. Vinattieri, F. Martelli, Y.-L. Chang, J. Merz, and S.-S. Stone, in *Proceeedings of XII International Conference on the Physics of Semiconductors, Vancouver, 1994* (World Scientific, Singapore, 1994), Vol. 2, pp. 1043–1046.
[12] D. Y. Oberli, J. Shah, T. C. Damen, C. W. Tu, T. Y. Chang, D. A. B. Miller, J. E. Henry, R. F. Kopf, N. Sauer, and A. E. Di Giovanni, Phys. Rev. B **40**, 3028 (1989).
[13] M. G. W. Alexander, W. W. Ruhle, R. Sauer, and W. T. Tsang, Appl. Phys. Lett. **55**, 885 (1989).
[14] B. Deveaud, F. Clerot, A. Chomette, A. Regreny, R. Ferreira, G. Bastard, and B. Sermage, Europhys. Lett. **11**, 367 (1990).
[15] M. Nido, M. G. W. Alexander, W. W. Ruhle, T. Schweizer, and K. Kohler, Appl. Phys. Lett. **56**, 355 (1990).
[16] M. G. W. Alexander, M. Nido, W. W. Ruhle, and K. Kohler, Phys. Rev. B **41**, 12 295 (1990).
[17] T. Matsusue, M. Tsuchiya, J. N. Schulman, and H. Sakaki, Phys. Rev. B **42**, 5719 (1990).
[18] B. Deveaud, A. Chomette, F. Clerot, P. Auvray, A. Regreny, R. Ferreira, and G. Bastard, Phys. Rev. B **42**, 7021 (1990).
[19] M. Nido, M. G. W. Alexander, W. W. Ruhle, and K. Kohler, Phys. Rev. B **43**, 1839 (1991).
[20] Ph. Roussignol, M. Gurioli, L. Carraresi, M. Colocci, A. Vinattieri, C. Deparis, J. Massies, and G. Neu, Superlattices Microstruct. **9**, 151 (1991).
[21] Ph. Roussignol, A. Vinattieri, L. Carraresi, M. Colocci, and A. Fasolino, Phys. Rev. B **44**, 8873 (1991).
[22] R. Ferreira, P. Rolland, Ph. Roussignol, C. Delalande, A. Vinattieri, L. Carraresi, M. Colocci, N. Roy, B. Sermage, J. F. Palmier, and B. Etienne, Phys. Rev. B **45**, 11 782 (1992).
[23] D. Rosen, A. G. Doukas, Y. Budansky, A. Katz, and R. R. Alfano, Appl. Phys. Lett. **39**, 935 (1981); D. von der Linde, J. Kuhl, and E. Rosengart, J. Lumin. **24/25**, 675 (1981).
[24] M. B. Johnson and T. C. McGill, J. Appl. Phys. **63**, 2077 (1988).
[25] N. Sawaki, R. A. Höpfel, and E. Gornik, Appl. Phys. Lett. **55**, 1996 (1989).
[26] M. K. Jackson, M. B. Johnson, D. H. Chow, and T. C. McGill, Appl. Phys. Lett. **54**, 552 (1989).
[27] R. Strobel, R. Eccleston, J. Kuhl, and K. Kohler, Phys. Rev. B **43**, 12 564 (1991).
[28] R. Kumar, A. S. Vengurlekar, and S. S. Prabhu, Solid State Commun. **100**, 287 (1996).
[29] C. Piermarocchi, F. Tassone, V. Savona, A. Quattropani, and P. Schwendimann, Phys. Rev. B **55**, 1333 (1997).
[30] The f_1 frequency spectrum has been taken by blocking the second beam (f_2) in order to measure a signal not affected by the interaction between the two beams; in fact the nonlinear term (A5) has a Fourier component also at the fundamental frequencies f_1 and f_2.
[31] To obtain the theoretical prediction for $I(t)$, the calculated curves $\nu(t)$ are convoluted with the measured instrumental-response function of the streak-camera system.
[32] D. Robart, X. Marie, B. Baylac, T. Amand, M. Brousseau, G. Bacquet, G. Debart, R. Planel, and J. M. Gerard, Solid State Commun. **95**, 287 (1995).
[33] T. C. Damen, J. Shah, D. Y. Oberli, D. S. Chemla, J. E. Cunningham, and J. M. Kuo, Phys. Rev. B **42**, 7434 (1990).
[34] W. E. Spicer, Z. Liliental-Weber, E. Weber, N. Newman, T. Kendelewicz, R. Cao, C. McCants, P. Mahowald, K. Miyano, and I. Lindau, J. Vac. Sci. Technol. B **6**, 1245 (1988).
[35] L. He, H. Hasegawa, T. Sawada, and H. Ohno, J. Appl. Phys. **63**, 2120 (1988).
[36] V. Emiliani, Ph.D. thesis, Universitá degli studi di Roma, 1996.
[37] A. Tackeuchi, S. Muto, T. Inata, and T. Fujii, Jpn. J. Appl. Phys. Part 2 **28**, L1098 (1988).
[38] Y. Sugiyama, A. Tackeuchi, T. Inata, and S. Muto, Jpn. J. Appl. Phys. Part 2 **30**, L1454 (1991).
[39] *Spectroscopy of Semiconductor Microstructures*, Vol. 806 of *NATO Advanced Studies Institute Series B: Physics*, edited by G. Fasol, A. Fasolino, and P. Lugli (Plenum, New York, 1989), p. 535.